



Slurry Erosion Wear Resistance and Impact-Induced Phase Transformation of Titanium Alloys

Xiulin Ji¹ · Qinyu Qing¹ · Cuicui Ji¹ · Jiangbo Cheng² · Yingtao Zhang¹

Received: 2 February 2018 / Accepted: 5 April 2018 / Published online: 9 April 2018
© Springer Science+Business Media, LLC, part of Springer Nature 2018

Abstract

Erosion wear resistance and impact-induced phase transformation of titanium alloys TA2 (pure Ti), TC4 (Ti–6Al–4V) and TC11 (Ti–6.5Al–3.5Mo–1.5Zr–0.3Si) were investigated using a slurry jet tester. The slurry erosion wear resistance of TA2 is comparable to that of 304 stainless steel, especially at the impingement angle 90°. Although TC4 and TC11 have higher hardness, TA2 possesses the best erosion wear resistance except TC11 at 15°. With the increasing erosion time, the eroded surface hardness of TC11 at the impingement angle 90° increases and then decreases, while the volume loss rate drops in the first 15 min, then increases until 30 min, and then slightly decreases again. With XRD characterization and SEM observation, erosion-induced phase transformation from metastable β -phase to α -phase is proved on the surface of titanium alloy TC11. And the thickness of visible phase transformation layer is about 10 μm . Phase transformation influences the erosive wear mechanism of titanium alloys. At the impingement angle of 30°, the material removal of TC4 and TC11 can be described as micro-plowing and lip extruding, while plowing mark is not a typical surface morphology of TA2, indicating a better work-harden ability. So, stabilizing β -phase can be an effective way to improve the erosion wear resistance of titanium alloys.

Keywords Wear resistance · Slurry erosion · Microstructure evolution · Phase transformation · Titanium alloy

1 Introduction

Titanium and its alloys, because of their excellent strength-to-weight ratio, excellent corrosion resistance, and biocompatibility, are widely used in aerospace, automotive, power plant, maritime, and many other industries [1–3]. They are also used in marine and offshore applications as tube and shell heat exchangers, steam condensers, valves, pumps, and pipelines [3–5]. However, the wider use of titanium and its alloys is frequently retarded by their reputation for poor tribological behavior [4]. Aircraft, rockets, and other aeronautical engines are often subjected to severe erosion situations from sands, rains, or other solid particles in space [6]. And the blades made of titanium alloys used for turbochargers, air and hydraulic pumps, turbines and impellers, etc., are exposed to wear, mainly by erosion or cavitation erosion

[1]. In order to improve erosion resistance, different surface treatments were applied to titanium and its alloys, such as surface nitridation [1], laser surface treatment [7, 8], shot peening and multi-arc ion plating [9], physical vapor deposition (PVD) [10], and chemical vapor deposition (CVD) [11]. However, despite growing use of titanium and its alloys in marine and offshore applications, there are only a few investigations on their slurry erosion wear.

As we all know, slurry erosion wear is caused by a stream of a slurry mixture of solid particles in a liquid, usually water, and results in material damages and losses. The effects of slurry erosion parameters, such as impingement angle, impacting velocity, and corrosive medium, were investigated, as well as the hardness, microstructure, and composition of titanium alloys. Impacting velocity is the most significant controlling factor influencing the solid particle erosion wear of Ti–6Al–4V alloy followed by impact angle, microstructural variation, and size of erodent [12]. Reducing the impingement angle increases the weight loss of the Ti–6Al–4V [1]. The erosion rate of TC4 (Ti–6Al–4V) at 90° impinged angle is lower than that at 30° impinged angle [13]. Finite element analysis was used to model the erosion behavior in abrasive waterjet machining for Grade

✉ Xiulin Ji
xiulinji@gmail.com

¹ College of Mechanical and Electrical Engineering, Hohai University, Changzhou 213022, China

² College of Mechanics and Materials, Hohai University, Nanjing 210098, China

5 titanium alloy (Ti–6Al–4V), and the result indicates a significant variation of crater geometry for the impact of up to the first 17 particles, depending on impacting velocity and angle [14]. Corrosive medium is normally beneficial to improve the erosion resistance of titanium under a low impacting velocity. The combination of erosion and salt spray corrosion reduces the erosion rate of TC4 [13]. And CP-Ti has negligible weight loss which was more than one order of magnitude lower than that of stainless steels AISI 304L and 316L in a solution containing 10 wt% HCl [15]. The microstructure and the hardness significantly affect the erosion resistance of the alloy. An improvement in hardness favors a high erosion resistance [8], and the resistance increases in order with increasing hardness [16]. The microstructural features of Ti–6Al–4V influence the development of damage, with grain boundaries exhibiting lower resistance to damage than grains themselves [17]. The lamellar microstructure of Ti–6Al–4V alloy has excellent erosion resistance, followed by bimodal and equiaxed microstructures [12]. As for the alloy composition, the titanium alloys (Ti 5111, Ti–6Al–4V ELI, Ti–6Al–4V ELI/Ru) are believed to have greater erosion–corrosion resistance than CP-Ti [18]. However, the former literature is still not enough to obtain a clear understanding of the slurry erosion wear of titanium and its alloys. Moreover, some of the conclusions from different kinds of literature are contradictory. For example, erosion resistance of Ti–6Al–4V increased surprisingly when the hardness decreased for the lower amount of precipitated β -phase during aging in the $\alpha + \beta$ region [19].

On the other hand, titanium and its alloys possess comparable erosion resistance. TC4 with low hardness and good toughness exhibits much better erosion resistance than 1Cr11Ni2W2MoV steel [13]. The material loss rate for Ti–6Al–4V is significantly lower than for 4340 steel and silicon bronze in seawater–sand slurries [20]. The annealed Ti–6Al–4V titanium alloy shows resistance to the cavitation erosion of approximately 2.3–3.4 times higher than that of the considered standard steels (i.e., 41Cr4 alloyed steel and X5CrNi13-4 stainless steel) [21]. The solid particle erosion rate on carbon fiber–epoxy composite was 1.5 times of that on pure titanium at impingement angle 15° and increased to 5 times at impact angle 90° [22]. However, in another

case, titanium (ASTM Grade 2) showed slightly higher mass loss than stainless steel 316L [23]. So, further research work needs to be done to confirm the erosion behavior and the erosion resistance of titanium and its alloys.

In this paper, slurry erosion was studied for pure titanium and various titanium alloy samples using a jet erosion testing machine. Commercial pure titanium TA2, the most used biphasic titanium alloy TC4, and high-hardness titanium alloy TC11 were selected as target materials. Not only the impacting angle but also the duration times were studied for the slurry erosion wear of titanium and its alloys. In particular, the deformation-induced microstructure evolution was paid more attention in this work.

2 Experimental

2.1 Materials

Three typical titanium and its alloys TA2 (pure titanium), TC4 (Ti–6Al–4V), and TC11 (Ti–6.5Al–3.5Mo–1.5Zr–0.3Si) were used in this work. And AISI 304 stainless steel was also used for comparison. Table 1 presents the chemical compositions [24] of the test materials together with their hardness and densities. All of the as-received samples were cut into 10 mm \times 10 mm \times 10 mm size for the slurry erosive wear test.

2.2 Microstructural Characterization

Metallographic specimens were prepared by the standard mechanical polishing method. And a mixture solution of HF/HNO₃/H₂O with a ratio of 2:1:17 was used as the etching agent. Macrostructure and microstructure of the three sections were examined by Jiangnan XJG-05 horizontal optical microscope (OM) and Hitachi S-3400N scanning electron microscope (SEM). And the surface morphologies of the eroded samples were also observed using SEM. For the phase identification, X-ray diffraction (XRD) measurements of TC11 samples were made before and after slurry erosion with a Rigaku D/max 2500 PC using Cu K α radiation. Vickers hardness

Table 1 Chemical compositions, hardness, and densities of the test materials

Materials	Chemical compositions [24]	Hardness (HV)	Density (g/cm ³)
TA2	C \leq 0.08, Fe \leq 0.30, H \leq 0.015, N \leq 0.030, O \leq 0.250, other total \leq 0.40, balanced Ti	215.5	4.51
TC4	5.50 \leq Al \leq 6.75, 3.5 \leq V \leq 4.5, C \leq 0.08, Fe \leq 0.30, H \leq 0.015, N \leq 0.050, O \leq 0.200, other total \leq 0.40, balanced Ti	354.0	4.43
TC11	5.8 \leq Al \leq 7.0, 2.8 \leq Mo \leq 3.8, 0.8 \leq Zr \leq 2.0, 0.20 \leq Si \leq 0.35, C \leq 0.08, Fe \leq 0.25, H \leq 0.012, N \leq 0.050, O \leq 0.150, other total \leq 0.40, balanced Ti	365.3	4.48
304 SS	8.0 \leq Ni \leq 10.5, 18.0 \leq Cr \leq 20.0, C \leq 0.08, Mn \leq 2.0, P \leq 0.045, Si \leq 0.030, balanced Fe	204.8	7.93

measurements were made on a standard micro-hardness tester (HXD-1000TMC, China) at 100 g load and 15 s loading duration.

2.3 Slurry Erosion Testing

Prior to the erosion test, in order to assure an average surface roughness (R_a) below $0.1 \mu\text{m}$, the specimens were ground progressively down to the 1000 grade SiC grinding paper and finished by mechanical polishing with $2.5\text{-}\mu\text{m}$ diamond grinding paste. The samples were ultrasonically cleaned in acetone, air-dried in desiccators, and then weighed using an electronic microbalance with an accuracy of 0.1 mg before and after erosion tests. Slurry erosion tests were performed in a jet erosion testing machine with a slurry flow composed of water and $15 \pm 1 \text{ wt\%}$ of SiO_2 particles ($350\text{--}600 \mu\text{m}$) at an impact velocity of 15 m s^{-1} , as shown in our previous work [25]. The morphology of sand particles was also presented in Ref. [25]. After slurry erosion, the mass loss was converted into volume loss based on the densities of the samples, as listed in Table 1. Each test was repeated at least three times; the average values were reported here.

3 Results and Discussion

3.1 Microstructural Characterization

Figure 1 shows the metallographs of as-received TA2, TC4, and TC11. It can be observed that TA2 is composed of single α -phase, while the initial microstructures of TC4 and TC11 consist of α -phase and β -phase. The volume content of primary α -phase (white phase) is much more than that of β -phase in TC4 matrix, as shown in Fig. 1b. And the microstructure of TC11 is composed of interconnected equiaxed primary α -grains and lamellar transformed β -grains, as shown in Fig. 1c.

3.2 Effect of Impingement Angle

The weight loss of 304 SS is larger than that of titanium and its alloys at every impingement angle. The relationships between the volume losses and impingement angles are illustrated for TA2, TC4, TC11, and 304 SS in Fig. 2. The curves of erosion rate versus impingement angle (Fig. 2) show the peak erosion rate that occurred at the impingement angle 30° , indicating ductile erosion behavior for titanium and its alloys. Comparing the volume losses of both samples of TA2 and 304 SS (Fig. 2), the volume loss of TA2 was comparable to that of 304 SS at the impingement angles from 30° to 90° . In particular, TA2 shows better erosion wear resistance than 304 SS at 90° . The volume losses of TC4 and TC11 were higher than that of TA2, except the volume losses of TC11 at 15° and 60° . Because TC4 and TC11 have a higher hardness than that of TA2, as shown in Table 1, it is interesting that the erosion resistance decreased when the hardness increased.

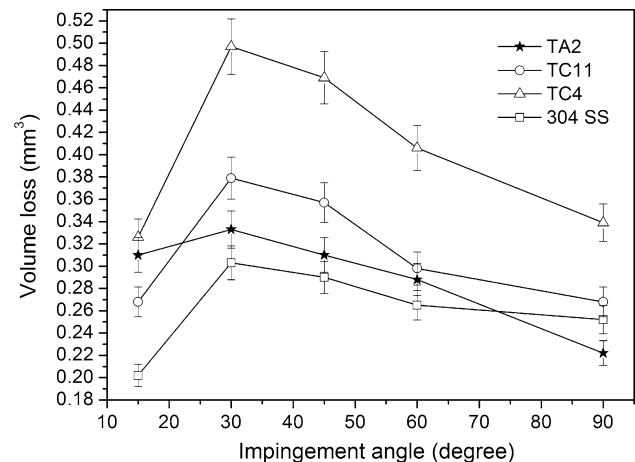


Fig. 2 Volume losses of TA2, TC4, TC11, and 304 SS with various impingement angles after 30-min erosion

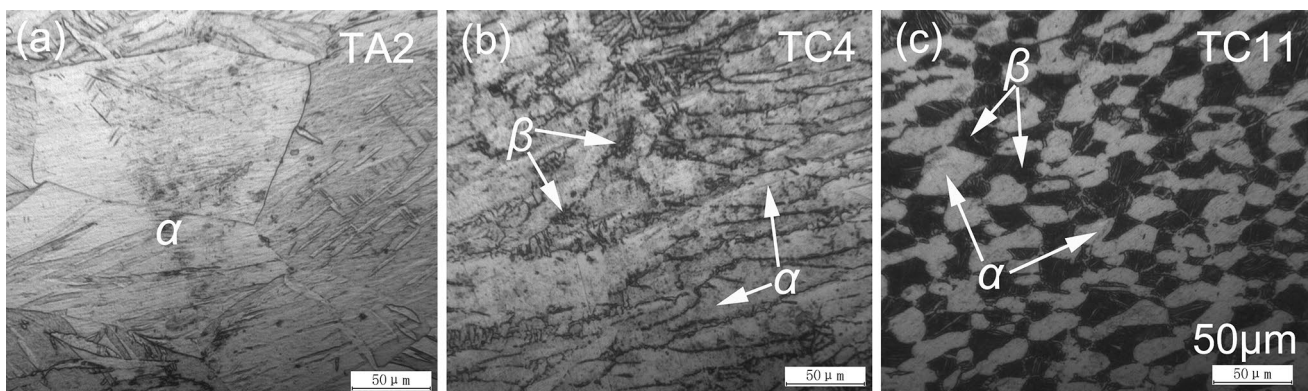
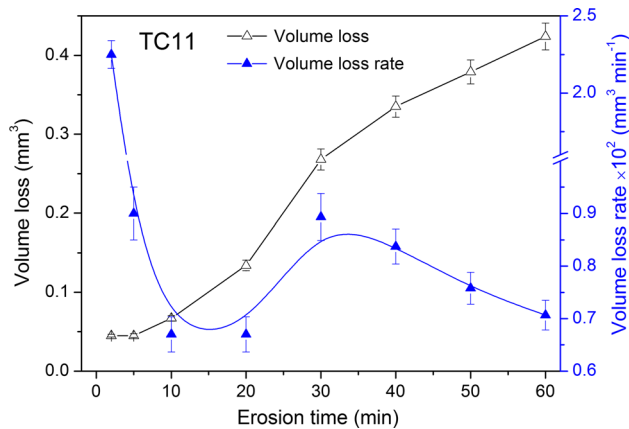


Fig. 1 Metallographs of as-received TA2, TC4, and TC11

Table 2 Mass loss, volume wear loss, and surface hardness of TC11 with the various erosion time

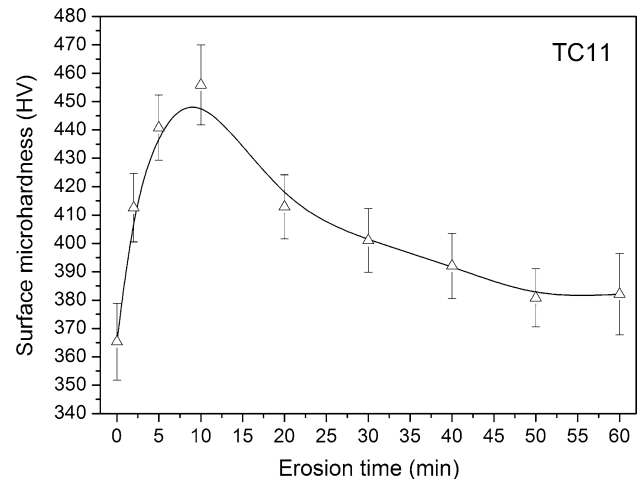
Erosion time (min)	0	2	5	10	20	30	40	50	60
Mass loss (mg)	/	0.2	0.2	0.3	0.6	1.2	1.5	1.7	1.9
Volume loss rate ($\text{mm}^3 \text{min}^{-1}$)	/	2.25	0.90	0.67	0.67	0.89	0.84	0.76	0.71
Surface hardness (HV)	365.3	412.6	440.8	455.9	412.9	401.0	392.0	380.8	382.1

**Fig. 3** Plots of the volume loss and the volume loss rate of TC11 samples as a function of duration at the impingement angle 90°

Similar results are also found in the erosion wear resistance of heat-treated Ti–6Al–4V alloy [19]. If TC4 is a typical plastic material for erosion, the volume loss of TC4 at 45° is supposed to be higher than those at 30° or 60° . However, the experimental results show the volume loss at 45° is lower than at both of them. The possible reason could be related to the balance between work hardening and phase transformation, and further work needs to be done on this unusual phenomenon.

3.3 Effect of Erosion Time

The volume losses of TC11 samples at the impingement angle 90° after different erosion time are listed in Table 2 and shown in Fig. 3. As can be seen, the volume loss always increases with the duration time. But the volume loss per minute drops in the first 15 min, then increases until 30 min, and then decreases again. Normally, the erosive wear rate decreases with the duration time because impingement of solid particles causes deformation-induced work hardening. The increase in volume loss rate at about 25 min indicates a change in wear mechanism. The surface micro-hardness was detected for the corresponding TC11 samples that eroded at a different time, as shown in Fig. 4. It increases with the duration and has the highest value at 10 min, which corresponds to the lowest volume loss rate. However, the hardness decreases after 10 min later, which suggests microstructure evolution or phase transformation during erosion.

**Fig. 4** Surface micro-hardness of TC11 as a function of duration during erosion at the impingement angle 90°

3.4 Phase Transformation

After 30-min erosion at 90° , the subsurface morphologies of TA2, TC4, and TC11 were observed via SEM, as shown in Fig. 5. It can be seen that the metallographic structure in a top surface layer of TA2 is distinctly denser and more refined compared with that of the matrix, indicating that severe plastic deformation occurs after erosion. The white phase (β -phase) disappears from the top layers of TC4 and TC11, suggesting a deformation-induced β to α phase transformation. Similarly, in the top layer of TC11 treated by ultrasonic impacting and rolling process (UIRP), the volume content of primary α -phase is more than that of β -phase in matrix [26]. Moreover, the thickness of visible plastic deformation and phase transformation layer is about 10 μm .

XRD patterns of TC11 that eroded after different time were obtained for an evidence of phase transformation, as shown in Fig. 6. Clearly, TC11 is composed of α and β phases. At the first 2-min erosion, the XRD pattern presents no evident difference with the original sample, indicating only deformation-induced work hardening in this initial stage. After longer erosion duration, the peaks corresponding to β -phase gradually faded away, as shown in Fig. 6, and almost disappeared after 20-min erosion. Semiquantitative XRD analysis [27] was used to estimate the quantities of β -phase, and the relative volume fraction of β -phase in the TC11 surface is 24, 20, 16, 13, and 12% at the erosion time

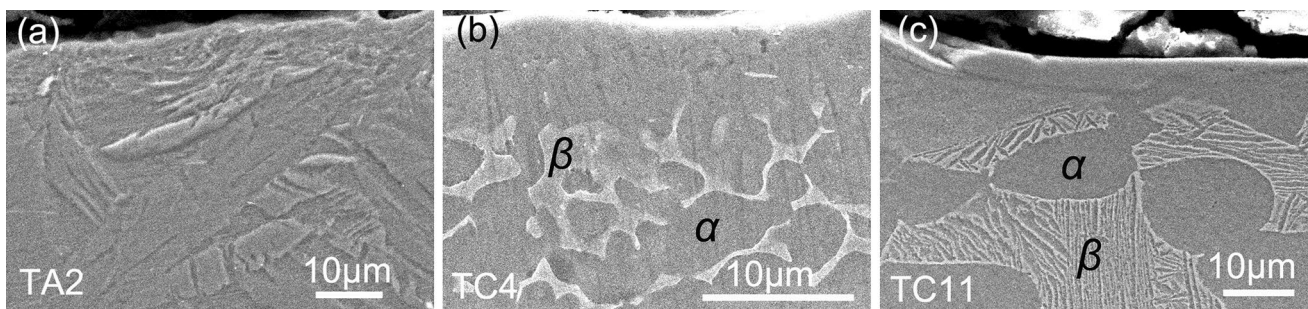


Fig. 5 Cross-sectional images for the subsurfaces of TA2, TC4, and TC11 after 30-min erosion at 90°

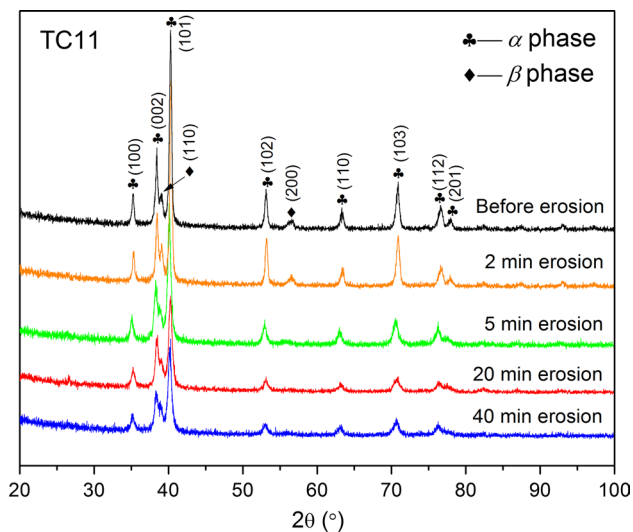


Fig. 6 XRD patterns of the eroded TC11 surface with various erosion times

of 0, 2, 5, 20, and 40 min, respectively. Therefore, erosion-induced phase transformation from metastable β -phase to α -phase is proved on the surface of titanium alloy. Furthermore, without hard β -phase, the surface hardness decreases (Fig. 4) and the volume loss rate increases (Fig. 3).

With Figs. 3, 4, 5, and 6, the interrelation between the erosion time and the variations of the volume loss rate and the surface hardness can be understood from the views of work hardening and phase transformation. At the first 15 min, because of work hardening, the surface hardness increases and the volume loss rate decreases. From 15 to 30 min, because of deformation-induced β to α phase transformation, the surface hardness decreases and the volume loss rate increases. After 30 min, the phase transformation of the retained β phase continues, which is confirmed by the decreasing diffraction peak intensity of $\beta(110)$. Meanwhile, the impact-induced grain refinement of α phase, which is proved by the broadening of X-ray diffraction peaks, causes the enhancement of strength and toughness. And it is beneficial to improve the erosion wear resistance. The complex

effect of phase transformation and grain refinement results in the slight decreases in the surface hardness and the volume loss rate.

3.5 Erosion Mechanism

Surface morphologies of slurry eroded TA2, TC4, and TC11 samples are shown in Fig. 7. At the impingement angle of 30°, the material removal of TC4 can be described as a micro-plowing process, as shown in Fig. 7b. Shorter grooves present in the eroded surface of TC11 and platelets and extruding lips increase, as shown in Fig. 7c. The difference between the two surface morphologies is reasonable for a higher hardness of TC11. However, multiple overlapping impacts with the formation of grooves and platelets present in the TA2 surface, while plowing mark is not a typical surface morphology of TA2, as shown in Fig. 7a. It is corresponding to the lower mass loss although its hardness is the lowest. This phenomenon indicates TA2 has a better work-hardening ability without the phase transformation of β -phase. Another reason could be attributed to the lower elastic modulus of TA2, which is a favor to absorb the impact energy of solid particles. Similar experimental results were also observed that the lower amount of precipitated β -phase during aging in the $\alpha + \beta$ region causes low hardness, but increases erosion resistance [19]. At the impingement angle of 90°, the surface morphologies of TA2, TC4, and TC11 are similar. And the craters, micro-cutting, and a few brittle fractures are typical morphologies of the eroded surface of titanium and its alloys.

4 Conclusions

Erosion wear resistance and surface microstructure evolution of TA2, TC4, and TC11 were investigated using the slurry jet tester. Within the limit tests of this study, the following conclusions can be drawn:

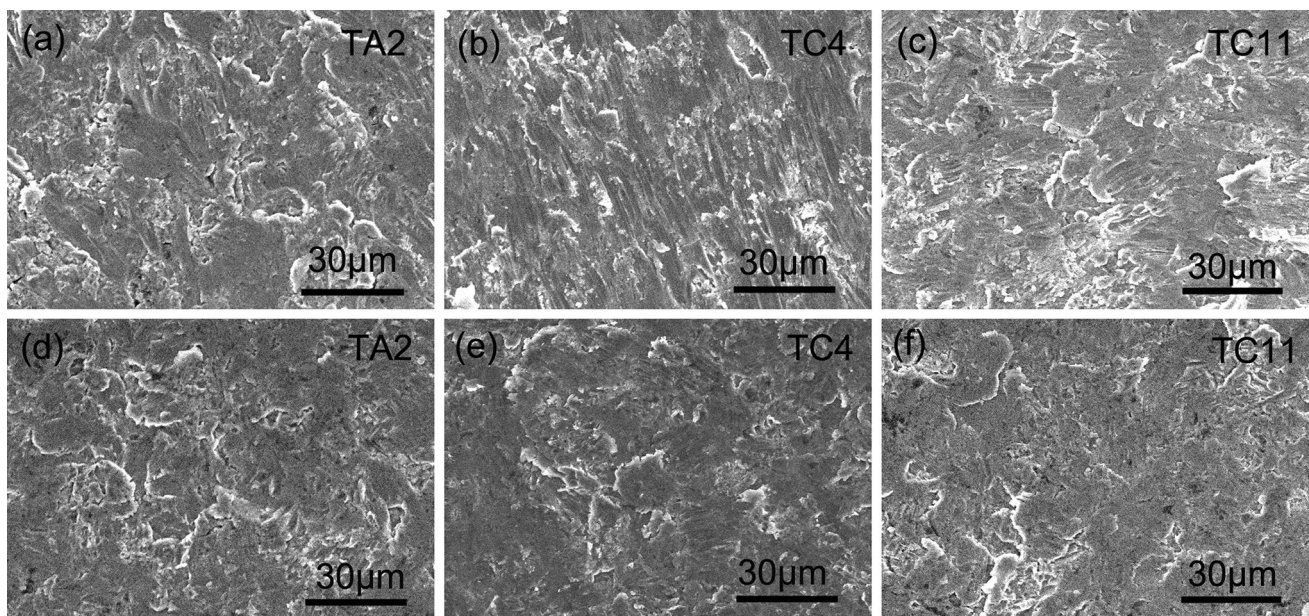


Fig. 7 Surface morphologies of eroded TA2, TC4, and TC11 samples at the impingement angle of 30° (a, b, c) and 90° (d, e, f)

1. The erosion wear resistance of TA2 is close to that of 304 SS at the impingement angles from 30° to 90°. Except for TC11 at 15°, TA2 possesses better erosion wear resistance than TC4 and TC11, though they have higher hardness.
2. With XRD characterization and SEM observation, erosion-induced phase transformation from metastable β -phase to α -phase is proved on the surface of titanium alloy. And the thickness of visible plastic deformation and phase transformation layer is about 10 μm .
3. Phase transformation influences the hardness and the wear resistance of titanium alloys. With the increasing erosion time, the eroded surface hardness of TC11 at the impingement angle 90° increases and then decreases, while the volume loss rate drops in the first 15 min, then increases until 30 min, and then slightly decreases again.
4. Phase transformation influences the erosive wear mechanism of titanium alloys. At the impingement angle of 30°, the material removal of titanium alloys can be described as a process of micro-plowing and lip extruding, while plowing mark is not a typical surface morphology of TA2, indicating a better work-harden ability.

Acknowledgements This research was supported by the National Natural Science Foundation of China (51475140, 51711530226).

References

1. Lisiecki, A., Kurc-Lisiecka, A.: Erosion wear resistance of titanium-matrix composite Ti/Tin produced by diode-laser gas nitriding. *Mater. Tehnol.* **51**(1), 29–34 (2017)
2. Ding, H.Y., Dai, Z.D., Zhou, F., Zhou, G.H.: Sliding friction and wear behavior of TC11 in aqueous condition. *Wear* **263**, 117–124 (2007). <https://doi.org/10.1016/j.wear.2007.01.106>
3. Khayatan, N., Ghasemi, H.M., Abedini, M.: Synergistic erosion–corrosion behavior of commercially pure titanium at various impingement angles. *Wear* **380–381**, 154–162 (2017). <https://doi.org/10.1016/j.wear.2017.03.016>
4. Dong, H., Bloyce, A., Bell, T.: Slurry abrasion response of surface engineered Ti6Al4VELL. *Tribol. Int.* **32**(9), 517–526 (1999). [https://doi.org/10.1016/S0301-679X\(99\)00082-1](https://doi.org/10.1016/S0301-679X(99)00082-1)
5. Chen, F.-J., Yao, C., Yang, Z.-G.: Failure analysis on abnormal wall thinning of heat-transfer titanium tubes of condensers in nuclear power plant Part II: Erosion and cavitation corrosion. *Eng. Fail. Anal.* **37**((Supplement C)), 42–52 (2014). <https://doi.org/10.1016/j.engfailanal.2013.11.002>
6. Fu, Y.Q., Du, H.J., Gu, Y.W.: Improvement of erosion resistance of titanium with different surface treatments. *J. Mater. Eng. Perform.* **9**(5), 571–579 (2000). <https://doi.org/10.1361/105994900770345719>
7. Mann, B.S.: Water droplet and cavitation erosion behavior of laser-treated stainless steel and titanium alloy: their similarities. *J. Mater. Eng. Perform.* **22**(12), 3647–3656 (2013). <https://doi.org/10.1007/s11665-013-0660-6>
8. Duraiselvam, M., Galun, R., Wesling, V., Mordike, B.L., Reiter, R., Oligmuller, J., Buvanashakaran, G.: Improvement of the cavitation erosion resistance of Ti–6Al–4V through laser alloying

- titanium aluminide based intermetallic matrix composites. *Lasers Eng.* **16**(5–6), 423–436 (2006)
9. Dong, H., Xing, L.D.: The research on the mechanism and prevention of solid particle erosion for titanium alloy. In: *Ti-2011: Proceedings Of the 12th World Conference on Titanium*, vol. Iii, pp. 1877–1880 (2012)
 10. Du, J., Zhang, P., Zhao, J.J., Cai, Z.H.: Erosion-resistant PVD ZrAlCuN coating for titanium alloy. *Adv. Compos. Pts 1 And 2* **150-151**, 51–55 (2011). <https://doi.org/10.4028/www.scientific.net/AMR.150-151.51>
 11. Grogler, T., Zeiler, E., Franz, A., Plewa, O., Rosiwal, S.M., Singer, R.F.: Erosion resistance of CVD diamond-coated titanium alloy for aerospace applications. *Surf. Coat. Technol.* **112**(1–3), 129–132 (1999). [https://doi.org/10.1016/S0257-8972\(98\)00800-7](https://doi.org/10.1016/S0257-8972(98)00800-7)
 12. Sahoo, R., Mantry, S., Sahoo, T.K., Mishra, S., Jha, B.B.: Effect of microstructural variation on erosion wear behavior of Ti–6Al–4V Alloy. *Tribol. Trans.* **56**(4), 555–560 (2013). <https://doi.org/10.1080/10402004.2013.767400>
 13. Shao, S., Xi, H.Z., Chang, Y.P.: Study on the Salt Spray Corrosion and Erosion Behavior of TC4 Titanium Alloy. *Fundamental Of Chemical Engineering, Pts 1–3*(233–235), 2409–2412 (2011). <https://doi.org/10.4028/www.scientific.net/AMR.233-235.2409>
 14. Kumar, N., Shukla, M.: Finite element analysis of multi-particle impact on erosion in abrasive water jet machining of titanium alloy. *J. Comput. Appl. Math.* **236**(18), 4600–4610 (2012). <https://doi.org/10.1016/j.cam.2012.04.022>
 15. Bermudez, M.D., Carrion, F.J., Martinez-Nicolas, G., Lopez, R.: Erosion-corrosion of stainless steels, titanium, tantalum and zirconium. *Wear* **258**(1–4), 693–700 (2005). <https://doi.org/10.1016/j.wear.2004.09.023>
 16. Mochizuki, H., Yokota, M., Hattori, S.: Effects of materials and solution temperatures on cavitation erosion of pure titanium and titanium alloy in seawater. *Wear* **262**(5–6), 522–528 (2007). <https://doi.org/10.1016/j.wear.2006.06.011>
 17. Huang, L., Folkles, J., Kinnell, P., Shipway, P.H.: Mechanisms of damage initiation in a titanium alloy subjected to water droplet impact during ultra-high pressure plain waterjet erosion. *J. Mater. Process. Technol.* **212**(9), 1906–1915 (2012). <https://doi.org/10.1016/j.jmatprotec.2012.04.013>
 18. Neville, A., McDougall, B.A.B.: Erosion- and cavitation-corrosion of titanium and its alloys. *Wear* **250**, 726–735 (2001). [https://doi.org/10.1016/S0043-1648\(01\)00709-8](https://doi.org/10.1016/S0043-1648(01)00709-8)
 19. Fidan, S., Avcu, E., Karakulak, E., Yamanoglu, R., Zeren, M., Sinmazcelik, T.: Effect of heat treatment on erosive wear behaviour of Ti6Al4V alloy. *Mater. Sci. Technol.* **29**(9), 1088–1094 (2013). <https://doi.org/10.1179/1743284713Y.0000000239>
 20. Yang, J., Swisher, J.H.: Erosion–corrosion behavior and cathodic protection of alloys in seawater-sand slurries. *J. Mater. Eng. Perform.* **2**(6), 843–850 (1993). <https://doi.org/10.1007/Bf02645684>
 21. Mitelea, I., Bordeasu, I., Utu, I.D., Karancsi, O.: Improvement of the cavitation erosion resistance of titanium alloys deposited by plasma spraying and remelted by laser. *Mater. Plast.* **53**(1), 29–33 (2016)
 22. Cai, F., Gao, F., Pant, S., Huang, X., Yang, Q.: Solid particle erosion behaviors of carbon-fiber epoxy composite and pure titanium. *J. Mater. Eng. Perform.* **25**(1), 290–296 (2016). <https://doi.org/10.1007/s11665-015-1848-8>
 23. Lindgren, M., Perolainen, J.: Slurry pot investigation of the influence of erodant characteristics on the erosion resistance of titanium. *Wear* **321**, 64–69 (2014). <https://doi.org/10.1016/j.wear.2014.10.005>
 24. Materia, T. <http://www.totalmateria.cn/>
 25. Ji, X.L., Han, X., Zhou, M.Y., Liu, J.Q.: Effect of heat treatment on the slurry erosion resistance of high strength steel DP980. *Int. J. Mater. Res.* **105**(5), 487–492 (2014)
 26. Zhao, X., Xue, G., Liu, Y.: Gradient crystalline structure induced by ultrasonic impacting and rolling and its effect on fatigue behavior of TC11 titanium alloy. *Results Phys.* **7**(Supplement C), 1845–1851 (2017). <https://doi.org/10.1016/j.rinp.2017.05.026>
 27. Davis, B.L.: Semiquantitative XRD analysis with the aid of reference intensity ratio estimates. *Powder Diffr.* **13**(3), 185–187 (2013). <https://doi.org/10.1017/S0885715600010083>